EARTH SCIENCES
RESEARCH JOURNAL
Earth Sci. Res. J. Vol. 29, No. 1 (March, 2025): 55 - 67

UNIVERSIDAD NACIONAL DE COLOMBIA

GEOTECHNICS

Landslide Distribution and Susceptibility Assessment in NW Pakistan: Insights from Field Observations and Factor Analysis

Mukhtar S. Ahmad[1],* Saad Khan[2], Nazir Ul Islam[3], Fazle Yar Khan[4], Imran Ahmad[5]
1. School of Earth and Space Sciences, Peking University, Beijing 100871, China; mukhtar@stu.pku.edu.cn
2. National Centre of Excellence in Geology, University of Peshawar, Peshawar 25130, Pakistan; saadkhan@uop.edu.pk
3. School of Earth Science and Resources, Chang'an University, Xi'an, Shaanxi 710054, China;nazirulislamgeo@gmail.com
4. Webuild,S.P.A Construction company Via Della Dataria Roma RM,Italy; f.khan@webuildgroup.et
5. Department of Geology, University of Malakand, Chakdara 18800, Dir (Lower), Pakistan, imran_geo@uom.edu.pk
*Corresponding Author: saadkhan@uop.edu.pk; saadkhan@geologist.com

ABSTRACT

The Hindukush region in Northwest Pakistan is a mountainous area that often faces natural disasters, such as landslides, flash floods, glacial lake outbursts, and debris flow, that alter the landscape and damage property. This study focused on the Chitral area of the Hindukush region to assess the landslide distribution and susceptibility using field observations and factor analysis. Nine landslide causative factors were selected and weighted using Geographic Information System (GIS)-based Frequency Ratio (FR) and Analytical Hierarchy Process (AHP) techniques. The factors included slope, aspect, rainfall, land cover, lithology, seismicity, distance to faults, streams, and roads. Landslide susceptibility maps were generated and classified into five categories: very high, high, moderate, low, and very low. Various landslides were observed in the field comprising debris flow, debris slide, soil erosion, and rockfall. Rockfall in the study area indicates active seismicity in the Hindukush region. Furthermore, the area under the curve method validated the results, which gave 0.80 for FR and 0.73 for AHP. The results showed that most of the landslides in the study area were caused by steep slopes of mountains, followed by precipitation. The high landslide susceptibility zones in the study area matched well with the field-based landslide collections, which showed the reliability of the mapping methods. These findings can help plan and implement measures in the Hindukush region to reduce the risk and impact of landslides, such as early warning systems, slope stabilization, land use regulation, and evacuation plans.

Keywords: Hindukush; Chitral; Susceptibility; Landslide; Inventory

Evaluación de la distribución y susceptibilidad de deslizamientos de tierra en el noroeste de Pakistán: perspectivas derivadas de observaciones de campo y análisis factorial

RESUMEN

La región de Hindukush en el noroeste de Pakistán es una área montañosa que eventualmente presenta desastres naturales, como deslizamientos de tierra, riadas, inundación por desborde de lagos glaciares y flujo de detritos, que alteran el paisaje y dañan la propiedad. Este estudio se enfoca en el área de Chitral, de la región Hindukush, con el fin de medir la distribución de los deslizamientos de tierra y la susceptibilidad a estos a través de observaciones de campo y análisis de factores. Para esto se seleccionaron nueve factores determinantes y se ponderaron a través de técnicas de relación de frecuencias y proceso de jerarquía analítica con base en sistemas de información geográfica. Estos factores son: inclinación, aspecto, precipitación de lluvia, cobertura terrestre, litología, sismicidad, distancia a fallas, arroyos y carreteras. Los mapas de susceptibilidad de deslizamientos se generaron y clasificaron en cinco categorías: muy alto, alto, moderado, bajo y muy bajo. Varios deslizamientos se observaron en campo para analizar el flujo de detritos, el deslizamiento de detritos, la erosión del suelo y la caida de rocas. La caida de rocas en el área de estudio indica la seismicidad activa en la región del Hindukush. Además, el área bajo el método de curva validó los resultados, con 0.80 para la relación de frecuencias y 0.73 para el proceso de jerarquía analítica. Los resultados señalan que los factores que han causado la mayoría de los deslizamientos de tierra en el área de estudio son las pendientes pronunciadas de las montañas y la precipitación. Las zonas de alta susceptibilidad a deslizamientos de tierra en el área de estudio coinciden con las colecciones de información de campo sobre deslizamientos, lo que muestra la fiabilidad de los métodos de mapeo. Estos hallazgos pueden ayudar a planear e implementar medidas en la región del Hindukush para reducir el riesgo y el impacto de los deslizamientos, tales como sistemas de alerta temprana, estabilización de taludes, regulación del uso del suelo y planes de evacuación.

Palabras clave: Hindukush; Chitral; susceptibilidad; deslizamientos de tierra; inventario

Record
Manuscript received: 05/12/2024
Accepted for publication: 05/03/2025

How to cite item:
Ahmad, M. S., Khan, S., Islam, N. U., Khan, F. Y., & Ahmad, I. (2025). Landslide Distribution and Susceptibility Assessment in NW Pakistan: Insights from Field Observations and Factor Analysis. *Earth Sciences Research Journal, 29*(1), 55-67. https://doi.org/10.15446/esrj.v29n1.117884

1. Introduction

Landslides are common and destructive natural hazards in mountainous regions worldwide (Khattak et al. 2010). Landslides have become more frequent in recent years due to rapid urbanization and population growth in undeveloped and developed countries. To mitigate landslide casualties, modern remote sensing and geographic information techniques and high-resolution data are essential for hazard analysis, risk assessment, and susceptibility mapping (Shafri et al. 2010; Khan et al. 2020; Ahmad et al. 2022). These techniques and data can assist in generating inventory maps of landslides that provide systematic information about the locations, types, and distribution of mass movements in an area (Xu et al. 2023; Ray et al. 2020). Moreover, these techniques and data can be used as the primary basis for generating thematic maps of geoenvironmental variables known as landslide causal factors (Basharat et al. 2016; Ahmad et al. 2023).

Reliable landslide analysis and the development of accurate landslide susceptibility maps depend on using suitable methods to assess the impact of various causal factors on landslide occurrence (Tang et al. 2020). These methods can help evaluate the influence of factors such as soil type, slope gradient, land cover, rainfall patterns, and geological characteristics on the likelihood of landslides. By analyzing and integrating these diverse factors, a comprehensive understanding of the spatial distribution and vulnerability of areas prone to landslides can be achieved. The detailed susceptibility maps support land-use planning, disaster management, and risk reduction efforts. By considering the complex interplay between causal factors and landslide occurrences, policymakers and stakeholders can make informed decisions to protect lives, infrastructure, and ecosystems from the devastating impact of landslides.

Various methods have been applied for landslide susceptibility, indicating the usefulness of qualitative and quantitative analysis methods, depending on the specific context, available resources, and desired outcomes (Basharat et al. 2016; Zêzere et al. 2017; Zhang et al. 2022; Ahmad et al. 2024). Landslide susceptibility analysis using statistical, InSAR, machine learning, and knowledge-based methods has been conducted by many researchers worldwide (Kaur et al. 2023; Agrawal and Dixit, 2023; Saha et al. 2023; Aslam et al. 2023, Wu et al. 2024, Ahmad et al. 2024). Among different methods, Frequency Ratio (FR) and Analytical Hierarchy Process (AHP) are preferred over complex machine learning techniques that require programming knowledge for landslide susceptibility mapping (Boukhres et al. 2023). FR and AHP methods are simple to understand and implement, making them accessible to researchers, practitioners, and decision-makers who may not have advanced programming skills or technical expertise. These methods provide transparent and interpretable results, enabling stakeholders to comprehend the factors influencing landslide susceptibility. This transparency is crucial in disaster management and land-use planning, where explainability is highly valued. FR and AHP methods can handle limited data availability, unlike complicated machine learning approaches that often demand large training datasets. FR employs basic statistical calculations based on historical landslide occurrences and conditioning factors (Razavizadeh et al. 2017, Youssef et al. 2023), while AHP incorporates expert judgment and pairwise comparisons, making them suitable for areas with sparse or incomplete data. AHP explicitly integrates expert knowledge and preferences through pairwise comparisons, allowing domain experts to contribute valuable insights and judgments (Saaty, 2004). This integration enhances the accuracy and reliability of susceptibility mapping.

In contrast, machine learning methods heavily rely on training data and may not consider expert inputs explicitly. FR and AHP methods are time and computationally efficient compared to complex machine learning algorithms. Machine learning models often involve resource-intensive computations, hyperparameter tuning, and extensive model training (Mao et al. 2024). FR relies on straightforward calculations, while AHP's pairwise comparisons can be performed relatively quickly. Although FR and AHP methods may not achieve the same predictive accuracy as advanced machine learning models in some cases, they have demonstrated reasonably good performance in landslide susceptibility mapping across various geographic regions. They offer valuable insights for decision-making purposes, even if they may not match the predictive capabilities of complex machine learning algorithms.

The northern Pakistan Himalayan-Hindukush-Karakoram belt is a region highly susceptible to landslides. The main factors that trigger landslides in this region are rugged topography, climate, geology, active tectonics, and infrastructure development on unstable slopes. It is estimated that nearly 30% of the world's slope movements occur in the steep and unstable slopes of the Himalayan region (Regmi et al. 2014; Du et al. 2020). The northern Pakistan Himalayan region is naturally unstable due to its geological conditions, steep slopes, high seismic activity, and monsoon rainfall (Khattak et al. 2010). Moreover, human activities such as road construction, urbanization, and deforestation can weaken the natural stability of slopes and trigger landslides (Aneel et al. 2023). This is particularly concerning given the region's rapid development and population growth. Considering these factors, landslide susceptibility mapping becomes essential for effective disaster management in Pakistan. By identifying areas prone to landslides, authorities can implement preventive measures, such as land-use planning, early warning systems, and infrastructure design considerations. It allows policymakers, planners, and engineers to make informed decisions to mitigate risks and protect lives and properties. The 2005 Kashmir earthquake is a stark reminder of northern Pakistan's urgent need for landslide susceptibility mapping. The earthquake triggered numerous landslides, causing widespread destruction and loss of life. Such events highlight the importance of understanding and managing landslide hazards in this highly susceptible region.

Our study evaluates landslides' spatial patterns and factors in the Chitral Area of the Hindukush region in Pakistan, a region prone to landslide hazards. We use field observations to create a geospatial dataset and analyze it with GIS-based FR and AHP techniques. Our study aims to enhance the understanding of landslide susceptibility in this region and inform effective mitigation strategies. Our research offers several novel contributions. First, based on field observations and factor analysis techniques, it provides a detailed analysis of the landslide distribution and vulnerability in the Hindukush region of Chitral in northwest Pakistan. This analysis reveals the areas at high risk of landslides and the main factors influencing their occurrence. This information is essential for designing and implementing measures to reduce the region's impact and risk of landslides. Second, our study compares the performance of two straightforward and transparent methods, FR and AHP, for landslide susceptibility mapping. We show that these methods can produce reasonably accurate results even with limited data availability. These findings make FR and AHP appealing to researchers, practitioners, and decision-makers who may lack advanced programming skills or technical expertise for machine learning modeling of landslide susceptibility.

2. Materials and Methods

2.1. Study Area

Chitral, a district in the Eastern Hindukush mountainous region of NW Pakistan, spans an area of 14,850 km². The district is geographically bordered by Afghanistan to the northwest, Gilgit to the east, and Dir and Swat to the south (Figure 1). Chitral is characterized by steep slopes, rugged terrain, and towering peaks reaching approximately 6000 m, which remain snow-covered throughout the year. The Mastuj River is the primary river that flows through Chitral and is fed by various tributaries. The climate in this region is warm during summers, cold during winters, and experiences snowfall in winter. The study area of Chitral is located within a tectonically active zone, where two continental plates collided during the Cretaceous-Eocene period, giving rise to the Himalayan Mountain range. The Tirich Mir Suture Zone (TMSZ) became active in the mid-Cretaceous. During the middle Jurassic, the Tirich Mir Fault reactivated as a south-verging fault, facilitating the exhumation of the Tirich Mir pluton to the surface. This pluton intersected the Tirich Mir mélange zone (Zanchi et al. 2000; Hildebrand et al. 2001; Saleem et al., 2021). Apatite fission track analysis and dating of the Tirich Mir pluton, conducted around 1.4 ± 0.5 million years ago, provided evidence of ongoing exhumation and uplift of the 7708 m Tirich Mir peak. In the late Cretaceous, the Kohistan Island Arc (KIA) collided with the southern margin of the Eurasian plate, forming the Shyoke Suture Zone (Khan et al. 2000; Fraser et al. 2001). Subsequently, after the closure of the Tethys Ocean, the Kohistan Island Arc collided with the Indian Plate along the Indus suture zone. Based on the structural evolution and stratigraphic record, the Chitral region in the Hindu Kush ranges is divided into three major tectonic units: i) the northwest unit between the Reshun fault and the Pakistan-Afghan border, ii) the central unit located between the northern suture and Reshun fault, and iii) the Kohistan unit situated between the Main Mantle Thrust and the

northern suture. Stratigraphically, the Chitral region consists of Paleozoic to Tertiary rocks within these three tectonic units, including granitic plutons. The stratigraphic sequences comprise the Charun Quartzite from the Devonian age, Shogram Formation, Reshun Formation from the Jurassic to Cretaceous age, Chitral Slates from the Cretaceous age, Lun Shale from the Carboniferous to Permian age, and various Igneous Plutons (Zanchi et al. 2000).

2.2. Data

The current study adopted various techniques and steps regarding literature review, field observation, and remote sensing to prepare the landslide susceptibility map (Figure 2). The literature data were collected from the various research catalogs and archives of the Geological Survey of Pakistan (GSP) and the Pakistan Meteorological Department (PMD). The following maps were constructed from the data collected: Landslide inventory map, prepared from Google Earth images using GIS; Geological map, digitized from geological map of Chitral; Seismological map, created from the USGS Earthquake Catalogue dataset (https://earthquake.usgs.gov/earthquakes/search/) of Chitral region; Rainfall map, created by utilizing the rainfall data of Chitral Drosh station. Structural features and lithology were modified from the geological map of Khan et al. (2000).

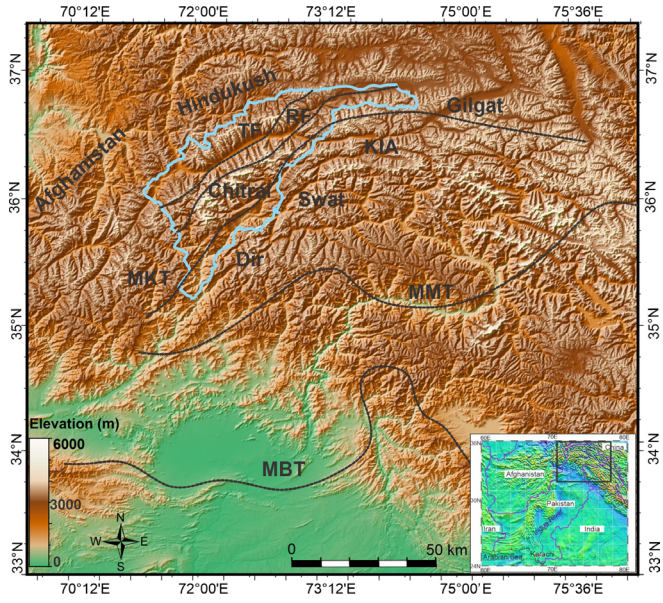

Figure 1. Map depicting the location of the study area in black polygon with regional tectonic elements MKT; Main Karakoram Thrust, TF; Tirich Mir Fault, RF; Reshun Fault, KIA; Kohistan Island Arc, MMT; Main Mantle Thrust, MBT; Main Boundary Thrust in black dashed line, inset map reflecting the study area over Pakistan map.

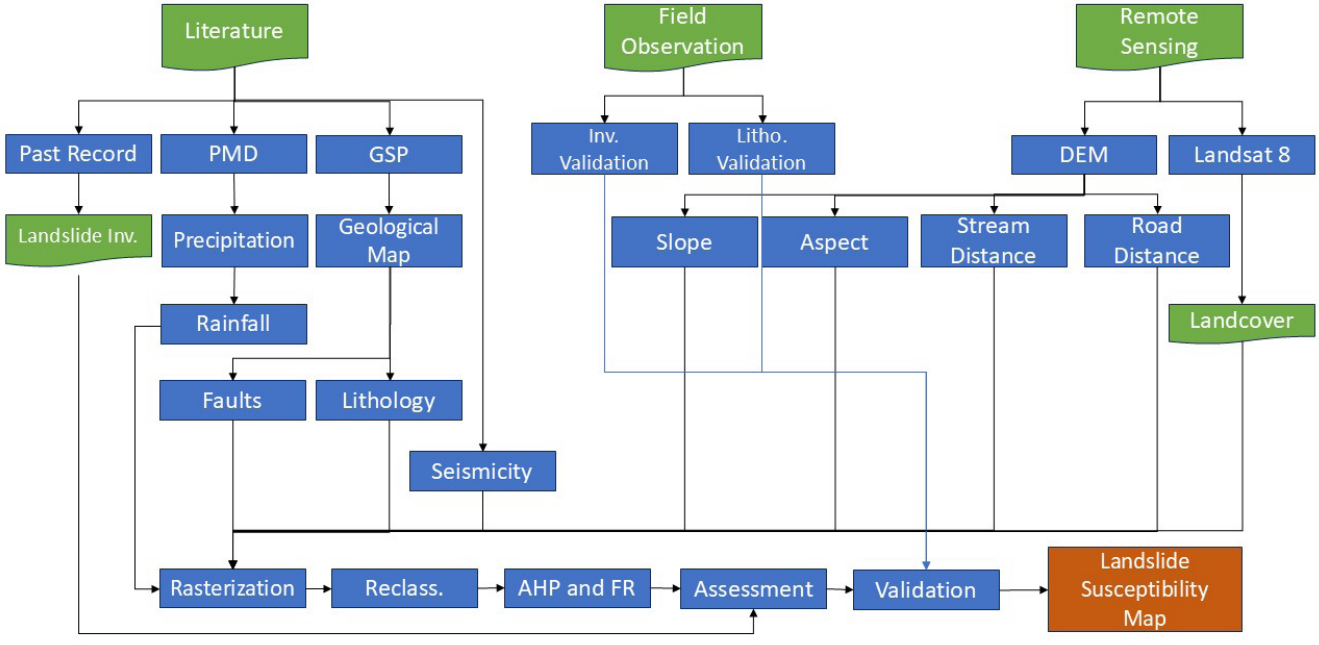

Figure 2. Methods and data set used for this research. PMD=Pakistan Meteorological Department, GSP= Geological Survey of Pakistan, DEM= Digital Elevation model.

2.2.1. Field Observation

During the field visit, various lithological units and geological structures, such as faults and locations of the landslides, were adequately examined. Furthermore, types, sizes, locations, failure mechanisms, and structural mechanisms were determined in the field to prepare a landslide inventory map for the Chitral Area. Such kind of maps are constructed to record and define the size of landslides in various areas, to examine the influence of the lithological unit's geological features (e.g., fold, faults, and fractures) on landslide occurrence and distribution, and to use it for making landslide zonation maps (Guzzetti et al. 2012;). The preparation of inventory maps includes several techniques based on satellite datasets, field observation, and data gathering from previous articles (van Westen et al. 2006). Field observation data and Google Earth images were used in this study to construct an inventory map for landslides along the road section. Polygon shapes for openly visible landslides on the satellite imagery were drawn from Google Earth, followed by confirmation in a field visit (Figure 3).

2.2.2. Remote Sensing

Various factors such as slopes, aspect, and distance to streams were derived from NASA SRTM (Shuttle Radar Topography Mission) based DEM of 30 m resolution (doi: 10.5066/F7PR7TFT). For the land cover map, Landsat-8 Satellite images of 2019 were retrieved from USGS on 21-02-2021 (https://lpdaac.usgs.gov) and classified based on supervised classification. The various thematic layers were constructed and further categorized by following the natural break classification method in GIS. Geomorphic factors like slope and slope aspect were created and categorized by adopting the natural break classification method in GIS. DEM imageries were used to extract the stream pattern using the Arc Hydro technique (Ahmad et al. 2023). The distance to the fault and lithology maps was digitized from already published geological data. Seismicity maps were constructed from the earthquake catalog data. Vector layers of fault distance and distance to stream, lithology, and a seismic map were then rasterized. The annual rainfall data were incorporated to construct a rainfall map. The landcover thematic layer was created from Landsat 8 images (https://lpdaac.usgs.gov/).

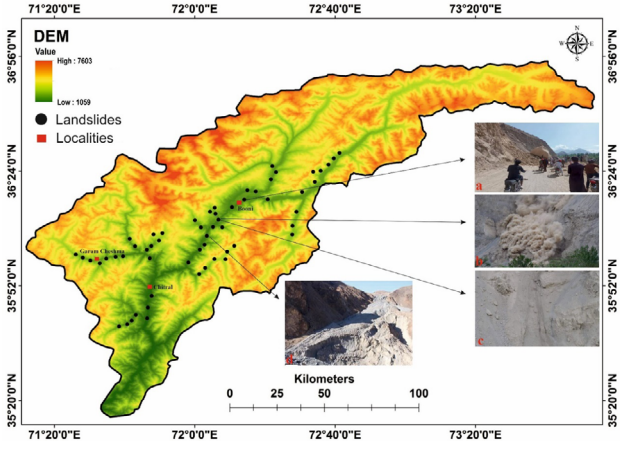

Figure 3. Landslide inventory map of Chitral area. Black points show the landslide locations observed in the field and on Google Earth. (a) Active rock fall near Mastuj captured during field visit, (b) landslide in Reshun area, (c) active remanence of Reshun landslide, and (d) active debris flow near Zaith village.

2.3. Methods

2.3.1 Analytical Hierarchy Process (AHP)

AHP modeling of landslide susceptibility is based on expert assessment to evaluate and weigh the causal factors using pairwise comparisons (Yalçın et al., 2011; Ahmad et al., 2023). Each factor is given a value from 1-9 depending on its relative importance, increasing influence from 1 to 9 (Table 1) (Saaty, 2004). The score given to factors is based on field observation, spatial data analysis, and operator expertise. If the factor on the x-axis is much more important than the one on the y-axis, then the value ranges between 1 and 9. The consistency ratio (CR) is used to control and avoid inconsistencies and biases in the whole process of ranking the causal factors (Bachri and Shresta, 2010; Yalçın et al. 2011)

$$CR = CI/RI \quad (1)$$

RI represents the random consistency index, while CI defines the consistency index shown in Eq. (2).

$$CI = \lambda Max - 1/(n-1) \quad (2)$$

where λMax is the calculation of the maximum eigenvalue and n represents a number of governing factors involved.

Table 1. Scale for pairwise comparisons [19].

Intensity of Importance	Explanation	Intensity of Importance	Explanation
1	Equal Importance	6	Strong Plus
2	Weak or Slight	7	Very strong
3	Moderate Importance	8	Very very strong
4	Moderate Plus	9	Extreme Importance
5	Strong Importance		

2.3.2. Frequency Ratio (FR)

FR is among the most widely used and popular approaches to assess landslide susceptibility (Thapa and Bhandari, 2019). The FR approach can quantify the relative influence degree of each attribute class of causal factors on the occurrence of landslides and reflect the response relationship between landslides and essential causal factors (Thapa & Bhandari, 2019; Zhang et al. 2020). A higher ratio indicates a stronger correlation between a causal factor and landslides. If FR values exceed 1, the corresponding causal factors favor increased landslide occurrence. If FR values are very close to 1, the relationship between environmental conditions and the occurrence of landslides in the relevant factor class is weak. Landslides are not expected to occur in this class range if FR values are below 1. The frequency ratio is based on the observed relationship between the spatial distribution and causative factors of landslides and can be expressed mathematically as in equation 3:

$$FR = \frac{\frac{Npix(LXi)}{\sum_{i=1}^{m} Npix\,(LXi)}}{Npix\,(Xj)/\sum_{j=1}^{n} N\,pix\,(Xj)} \quad (3)$$

In the equation, FR represents the frequency ratio for class i parameter j, whereas ***Npix*(*LXi*)** represents the pixel numbers of landslides in class i of the parameter variable. And ***Npix* (*Xj*)** is the number of pixels in parameter variable Xj. M represents the class number in the parameter variable Xi, and n reflects the parameters in the study region.

In step 2, FRs were kept normalized in the range of (0,1) probability values as a Relative Frequency. The RF was computed for each class using Equation 4.

$$RF = FRij/\sum_{i=1}^{m} FRij \quad (4)$$

After normalization, relative frequency still carries some drawbacks in considering all training factors as equal weight. To assess the shared interrelationship between the independent variables and suppress the drawback, the prediction rate (PR) was computed for rating each factor with the training dataset, as shown in equation 5.

$$PR = \frac{(RFmax - RFmin)}{(RFmax - RFmin)} \quad (5)$$

In the last step, Landslide susceptibility was generated by summing the product of PR of each factor and RF of each class as represented in equation 6.

$$LSI = \sum(PR * RF) \quad (6)$$

2.3.3. Accuracy Assessment and Comparison

Accuracy assessment is a necessary element after the construction of the landslide susceptibility map. The previous researchers have employed various statistical methods to check the accuracy of susceptibility maps such as LDA (Landslide Density Analysis), PRC (Prediction Rate Curve), ROC (Receiver Operating Curve), and AUC (Area under Curve) (Yesilnacar and Hunter, 2005, Wang et al. 2020). In the current research, we used the AUC technique to evaluate the predictive accuracy of the susceptibility map. AUC is a product of a graphical representation of two operating classes, i.e., TPR (true positive rate) and FPR (false positive rate), to measure the accuracy of the project. (Figure 7). The X-axis represents the false predicted events FPR, whereas the Y-axis represents the TPR true predicted events. This type of curve describes the efficiency of a model (Vakhshoori and Zare, 2018, Kuradusenge et al. 2020). Depending on the accuracy model, the area under the curve can range from 0.5 to 1 for various cases. A value close to 0.5 shows random outcomes, whereas values close to 1 indicate a correct model (Hosmer et al., 2013).

3. Results

3.1. Landslides in Chitral Region

From the field observation, 58 landslides were detected and used to prepare the inventory map. The landslides observed in field data comprise shallow landslides, rock falls, rock avalanches, soil erosion, and debris flow. Three road sections (Ayun to Kilash Valley Road, Chitral-Garam Cheshma Road, and Chitral-Mastuj Road) were covered in the field and are affected by a large amount of mass wasting due to slope instability and heavy rainfall. Along these sections, traffic interruption and highway blockage are routine phenomena (Figure 3a). A large amount of debris flows along the Reshun Zaith road unit due to a steep slope and recent sediment. This section also experienced one of the massive landslides that blocked the Mastuj River in 2015 (Figure 3b). Along the main Garam Cheshma road, soil erosion and rock falls are present in large amounts, whereas Kelash Valley road experiences soil debris flow and a few landslides caused by rock falls.

3.2. Factor Analysis

The thematic maps of the landslide causal factors used in this study are shown in Figure 4. The results revealed that the distribution and size of the landslides vary locally, depending on the rank of factors considered in the study. The region consists of igneous, sedimentary, and metamorphic rock sequences, including slates, quartzite, carbonates, shale, and granitic plutons. Recent sediment shales and Chitral slates exhibit many rocks and debris erosion.

The main structural features of the Chitral Hindukush region are the Main Karakorum thrust, Reshun Fault, and Terich Mir Fault. Reshun and Main Karakoram Thrusts are almost parallel to some localities' river and road sections. Fault maps for the study area were classified into eight classes. Some of the detected landslides were situated within 1 km of the active geological faults, suggesting that these structures also firmly control landslide triggering in the study area (Figure 4b).

The Chitral region displays variation in topography consisting of steep to gentle slopes, elevated cliffs, and narrow and deep valleys. The results revealed that the landslides were correlated with these factors.

Regarding land cover landslide relationships, the results showed that most landslide-affected areas lay in barren and rocky areas, and grassland showed sparse landslide events.

In the study area, several minor streams feed the main Mastuj-Chitral River. The key debris flow source is the high energy water flow and discharge in streams during monsoon season. During the monsoon season, heavy rainfall triggers several landslides by increasing the pressure of pore water in loose, unconsolidated sediments (Wang et al., 2020; ReliefWeb, 2024).

The rainfall map indicated that the northern part of the Chitral region receives the most rainfall. In contrast, the lower area of Chitral receives low precipitation, resulting in more landslide occurrence in the northern part.

In the current study, distances to road maps were classified into seven classes with intervals of 400m. From the results, the >400m distance is more important than other classes, and this area is more susceptible to slope instability.

Hindu Kush, Karakoram, and Himalayas mountainous terrains are among the most seismically active regions in the world. Active seismicity of these regions is associated with the convergence of the Eurasian and Indian Plates. Several active structures in reverse and strike-slip faults exist in the terrains of the Hindu Kush region. The study area is bounded to the south by the Main Karakoram Thrust, Reshun Fault in the central part, and Tirich Mir Fault to the northwest of the study area (Figure 1). These structures have caused moderate to high earthquakes in the past and experience moderate earthquakes of 5 magnitude each year (Schurr et al., 2014). The earthquake zone map shows that the area between the Reshun Fault and the Main Karakoram Thrust is regarded as a highly active seismic zone.

An extensive factor analysis using the FR method showed that lithology has a leading role in the landslide distribution in the area with FR 13.75, followed by the slope factor with FR 7.94. Rainfall is ranked as the third factor for landslide susceptibility, whereas the rest are considered less critical for landslide distribution (Table 2).

The calculated CI was then compared with the RI taken from the table to find the CR value. The CR value represents the inconsistency in the expert's decision in weighting factors. A CR value of less than 0.1 indicates that the decision is consistent, whereas a larger 0.1 value indicates inconsistency. Subclasses of each factor were ranked by using a pairwise comparison technique. In the final phase, each factor was weighed upon completion of the method. The value of CR in the current study was 0.08, which is below 0.1, which indicates that the assessment and weighting criteria are consistent, balanced, and reliable (Table 3).

Table 2. Factor analysis using the FR method.

Factor	Classes	Class Pixels (%)	Landslide Pixels (%)	FR	RF
Slope	<10°	20.00	14.88	1.04	0.13
	10°-20°	18.00	15.16	1.18	0.15
	20°-30°	12.00	17.30	1.31	0.17
	30°-40°	14.00	18.04	1.51	0.19
	40°-50°	16.00	17.15	1.43	0.18
	50°-60°	8.00	9.38	0.79	0.10
	60°-70°	7.00	5.31	0.44	0.06
	>70°	5.00	2.79	0.23	0.03
		100.00	100.00	7.94	

(*Continued*)

Factor	Classes	Class Pixels (%)	Landslide Pixels (%)	FR	RF
Aspect	Flat	11.29	7.18	0.64	0.07
	north	11.14	8.83	0.79	0.09
	northeast	11.16	11.62	1.04	0.12
	east	11.31	13.82	1.22	0.14
	south east	11.24	14.47	1.29	0.14
	south	10.97	13.85	0.26	0.14
	southwest	10.97	12.67	0.16	0.13
	west	11.47	10.82	0.94	0.11
	north west	10.46	6.75	0.65	0.07
		100.00	100.00	6.99	
Rainfall	35-36	56.54	60.93	1.08	0.16
	37-36	4.22	3.77	0.89	0.13
	37-36	35.27	32.30	0.92	0.13
	37-36	0.41	0.51	1.25	0.18
	37-36	1.79	1.96	1.10	0.16
	37-37	0.21	0.33	1.55	0.22
	38-37	1.56	0.21	1.13	0.02
		100.00	100.00	7.91	
Distance to Road	0-400	6.79	3.76	0.55	0.12
	400-800	13.01	6.78	0.52	0.11
	800-1200	10.52	8.17	0.78	0.17
	1200-1600	8.31	8.20	0.99	0.22
	1600-2000	7.23	6.38	0.88	0.19
	>2400	54.14	66.70	1.23	0.27
		100.00	100.00	4.95	
Distance to River	0-500	6.50	6.74	1.04	0.13
	500-1000	6.59	6.65	1.01	0.12
	1000-`1500	6.14	6.50	0.06	0.13
	1500-2000	17.62	18.91	1.07	0.13
	2000-2500	14.77	16.19	1.10	0.13
	2500-3000	11.60	12.79	1.10	0.13
	3000-3500	8.83	9.44	0.07	0.13
	>3500	27.95	22.78	0.82	0.10
		100.00	100.00	6.27	
Distance to Fault	0-1000	8.00	13.66	0.94	0.13
	1000-2000	7.00	12.21	0.85	0.12
	2000-3000	6.00	25.39	1.77	0.25
	3000-4000	23.00	33.60	2.36	0.34
	4000-5000	14.00	11.86	0.83	0.12
	5000-6000	17.00	2.83	0.20	0.03
	>7000	25.00	0.45	0.03	0.00
		100.00	100.00	6.99	
Lithology	CS	9.28	4.74	0.51	0.04
	KS	2.27	0.09	0.04	0.00
	MI	4.54	2.25	0.50	0.04
	MZ	6.08	0.12	0.03	0.00
	PZ	4.26	3.70	0.40	0.03
	S	8.22	9.71	1.18	0.09
	TI	6.00	15.11	2.98	0.22
	TR	52.75	61.38	1.16	0.08
	TRMS	0.58	2.64	4.57	0.33
	TS	2.80	0.03	0.01	0.00
	PC	3.21	0.22	0.07	0.00
		100.00	100.00	13.75	

(*Continued*)

Factor	Classes	Class Pixels (%)	Landslide Pixels (%)	FR	RF
Earthquake	Very Low	34.24	35.98	1.05	0.26
	Low	20.77	19.78	0.95	0.24
	Moderate	22.03	20.86	0.95	0.23
	High	22.95	23.37	1.02	0.25
	Very high	0.01	0.00	0.08	0.02
		100.00	100.00	4.05	
Landcover	Crop land	9.28	4.74	0.51	0.04
	Grass Land	8.00	7.00	0.04	0.00
	Deciduous forest	4.54	2.25	0.50	0.04
	Evergreen forest	6.08	4.00	0.03	0.00
	Sparse Vegetation	7.26	1.70	0.40	0.03
	Bare land	25.00	24.00	1.18	0.09
	Flooded vegetation	4.63	6.00	0.98	0.22
	Urban area	20.00	35.00	1.16	0.08
	Water	0.21	2.30	2.57	0.33
	Rocky area	15.00	13.00	0.01	0.00
		100.00	100.00	7.38	

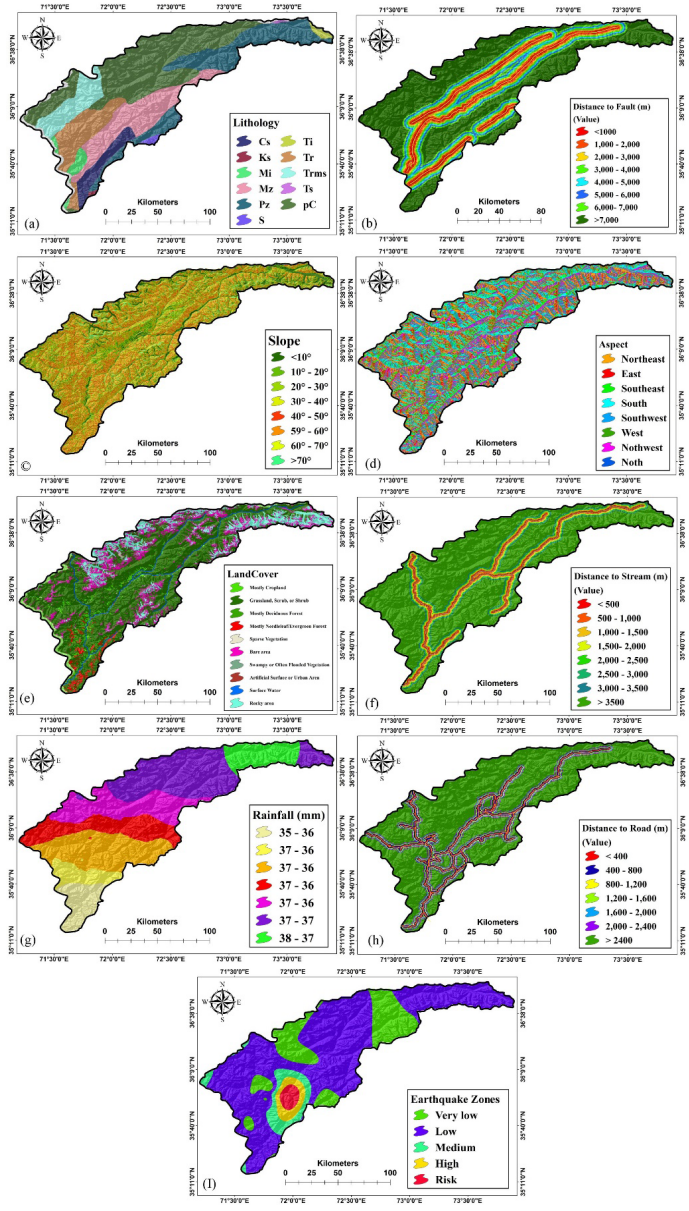

Figure 4. Landslide causative factors; (a) Lithology map (b) Distance to fault (c) Slope (d) Aspect (e) Land cover (f) Distance to stream (g) Rainfall (h) Distance to the road (i) Earthquake zones.

Table 2. Factor analysis using the FR method.

Factor	Classes	Class Pixels (%)	Landslide Pixels (%)	FR	RF
Slope	<10°	20.00	14.88	1.04	0.13
	10°-20°	18.00	15.16	1.18	0.15
	20°-30°	12.00	17.30	1.31	0.17
	30°-40°	14.00	18.04	1.51	0.19
	40°-50°	16.00	17.15	1.43	0.18
	50°-60°	8.00	9.38	0.79	0.10
	60°-70°	7.00	5.31	0.44	0.06
	>70°	5.00	2.79	0.23	0.03
		100.00	100.00	7.94	
Aspect	Flat	11.29	7.18	0.64	0.07
	north	11.14	8.83	0.79	0.09
	northeast	11.16	11.62	1.04	0.12
	east	11.31	13.82	1.22	0.14
	south east	11.24	14.47	1.29	0.14
	south	10.97	13.85	0.26	0.14
	southwest	10.97	12.67	0.16	0.13
	west	11.47	10.82	0.94	0.11
	north west	10.46	6.75	0.65	0.07
		100.00	100.00	6.99	
Rainfall	35-36	56.54	60.93	1.08	0.16
	37-36	4.22	3.77	0.89	0.13
	37-36	35.27	32.30	0.92	0.13
	37-36	0.41	0.51	1.25	0.18
	37-36	1.79	1.96	1.10	0.16
	37-37	0.21	0.33	1.55	0.22
	38-37	1.56	0.21	1.13	0.02
		100.00	100.00	7.91	
Distance to Road	0-400	6.79	3.76	0.55	0.12
	400-800	13.01	6.78	0.52	0.11
	800-1200	10.52	8.17	0.78	0.17
	1200-1600	8.31	8.20	0.99	0.22
	1600-2000	7.23	6.38	0.88	0.19
	>2400	54.14	66.70	1.23	0.27
		100.00	100.00	4.95	
Distance to River	0-500	6.50	6.74	1.04	0.13
	500-1000	6.59	6.65	1.01	0.12
	1000-`1500	6.14	6.50	0.06	0.13
	1500-2000	17.62	18.91	1.07	0.13
	2000-2500	14.77	16.19	1.10	0.13
	2500-3000	11.60	12.79	1.10	0.13
	3000-3500	8.83	9.44	0.07	0.13
	>3500	27.95	22.78	0.82	0.10
		100.00	100.00	6.27	
Distance to Fault	0-1000	8.00	13.66	0.94	0.13
	1000-2000	7.00	12.21	0.85	0.12
	2000-3000	6.00	25.39	1.77	0.25
	3000-4000	23.00	33.60	2.36	0.34
	4000-5000	14.00	11.86	0.83	0.12
	5000-6000	17.00	2.83	0.20	0.03
	>7000	25.00	0.45	0.03	0.00
		100.00	100.00	6.99	

(*Continued*)

Factor	Classes	Class Pixels (%)	Landslide Pixels (%)	FR	RF
Lithology	CS	9.28	4.74	0.51	0.04
	KS	2.27	0.09	0.04	0.00
	MI	4.54	2.25	0.50	0.04
	MZ	6.08	0.12	0.03	0.00
	PZ	4.26	3.70	0.40	0.03
	S	8.22	9.71	1.18	0.09
	TI	6.00	15.11	2.98	0.22
	TR	52.75	61.38	1.16	0.08
	TRMS	0.58	2.64	4.57	0.33
	TS	2.80	0.03	0.01	0.00
	PC	3.21	0.22	0.07	0.00
		100.00	100.00	13.75	
Earthquake	Very Low	34.24	35.98	1.05	0.26
	Low	20.77	19.78	0.95	0.24
	Moderate	22.03	20.86	0.95	0.23
	High	22.95	23.37	1.02	0.25
	Very high	0.01	0.00	0.08	0.02
		100.00	100.00	4.05	
Landcover	Crop land	9.28	4.74	0.51	0.04
	Grass Land	8.00	7.00	0.04	0.00
	Deciduous forest	4.54	2.25	0.50	0.04
	Evergreen forest	6.08	4.00	0.03	0.00
	Sparse Vegetation	7.26	1.70	0.40	0.03
	Bare land	25.00	24.00	1.18	0.09
	Flooded vegetation	4.63	6.00	0.98	0.22
	Urban area	20.00	35.00	1.16	0.08
	Water	0.21	2.30	2.57	0.33
	Rocky area	15.00	13.00	0.01	0.00
		100.00	100.00	7.38	

Table 3. Pairwise comparison between factors used in this study.

Pairwise comparison of Landslide Susceptibility Factors										
Factors	**Slope**	**Rainfall**	**Earthquiake**	**Lithology**	**Distance to Fault**	**Distance to Road**	**Landcover**	**Aspect**	**Distance to stream**	**Weight**
Slope	1	5	4	4	2	3	4	7	7	31.8015
Rainfall	0.2	1	2	4	5	3	6	5	6	20.6148
Eartquake	0.25	0.5	1	2	3	4	5	5	4	14.3954
Lithology	0.25	0.25	0.5	1	2	3	3	5	6	10.302
Distance to Fault	0.5	0.2	0.333333333	0.5	1	2	2	4	5	7.9474
Distance to Road	0.333333333	0.333333333	0.25	0.333333333	0.5	1	2	3	4	5.533
Landcover	0.25	0.16666667	0.2	0.333333333	0.5	0.5	1	2	4	4.2618
Aspect	0.142857	0.2	0.2	0.2	0.25	0.333333333	0.5	1	2	2.6566
Distance to stream	0.142857	0.16666667	0.25	0.16666667	0.2	0.25	0.25	0.5	1	2.0575
Consistency Ratio = 0.0851										

3.3 Landslide Susceptibility Map

We used a GIS-based weighted overlay technique to produce the landslide susceptibility maps based on the multi-class weighted factors. These susceptibility maps were further classified into five classes: very high, high, moderate, low, and very low susceptible zones (Figures 5-6).

The generated maps were validated using the ROC curve, which yielded an AUC value of 0.803 for the AHP model and 0.732 for the FR model (Figure 7).

4. Discussion

The current study adopted GIS-based AHP and FR methods to analyze landslide distribution and construct the susceptibility maps of the district Chitral Hindukush region. Nine landslide-triggering factors were considered for the generation of susceptibility maps. Assessment of the existing literature confirmed the causal factors responsible for triggering mass movement (Ahmad et al. 2023; Guzzetti et al. 2020). Subsequently, geospatial analysis was used to order and rank these factors. Slope, lithology, and rainfall were identified as basic environments for slope instability and valued as the most significant factors. The major influencing factor was slope, which triggered slope movements and failure. This was consistent with other studies that showed that steep slope regions in mountain terrains were more prone to collapse than gentle slope regions (Dai et al. 2001; Ghimire, 2011; Khan et al. 2020; Panday and Dong, 2021; Zou et al. 2021).

The distribution of rainfall in Pakistan varies on large scales. It's mainly related to the monsoon winds and disturbance of western regions like Iran and Afghanistan, but the precipitation does not occur throughout the year. For example, the northern mountains of Khyber Pakhtunkhwa and some parts of Baluchistan provinces receive heavy rainfall in winter, from December to March. In contrast, Sindh & Punjab receive 50-75% precipitation during the monsoon period. Monsoons are regarded as one of the primary rainfall sources in the whole Chitral district. Generally, glaciers and snow melting are primarily due to the rainfall spill that frequently occurs in summer. Rainfall is a major controlling factor for landslide occurrences (Ahmad et al. 2024).

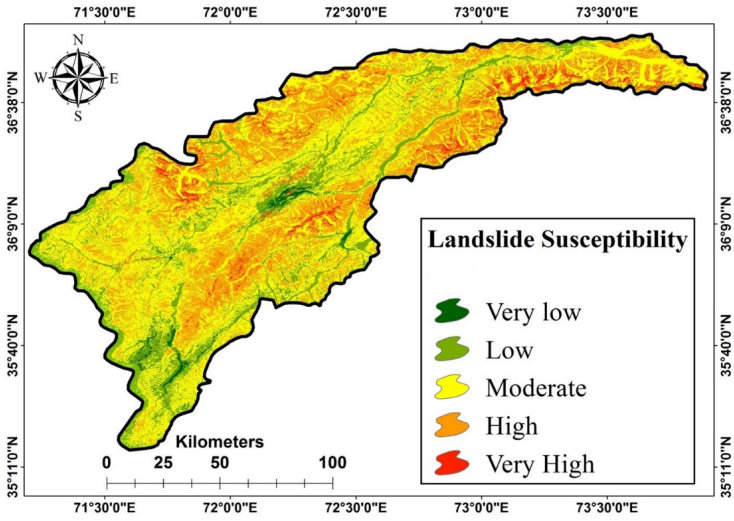

Figure 5. Landslide susceptibility map using the AHP method.

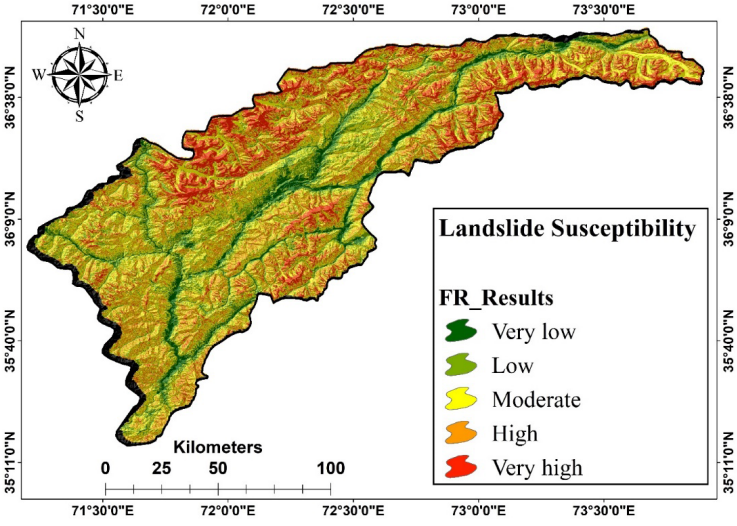

Figure 6. A landslide susceptibility map using the FR method.

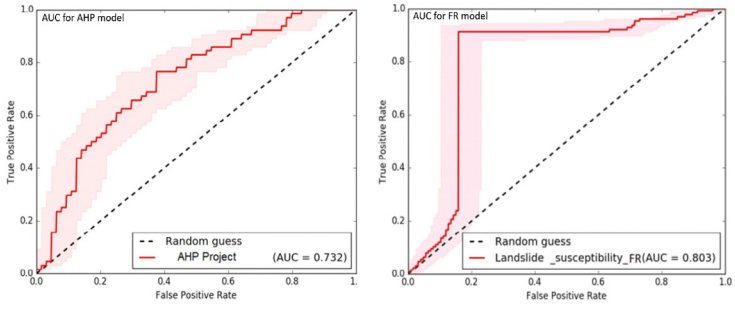

Figure 7. ROC curves and AUC values of the AHP and FR models

A data set's quality directly impacts the overall quality of the outcomes (Gorsevski et al., 2006). Among the fundamental and crucial data sets is the landslide inventory. Any inaccuracies about the location and recent movement of landslides can significantly undermine the accuracy of the final map. To address this issue, we conducted a study where we utilized satellite imagery to create a landslide inventory. Furthermore, field observations were performed to validate the identified landslide activity spots. All these thematic maps were further processed and compiled by AHP and FR methods. Many researchers used the AHP-based weighted overlay technique to prepare landslide susceptibility maps (Ahmed, 2015; Das et al. 2022; Ahmad et al. 2023). The accuracy of the final created map in the current project was 73% and regarded as suitable. The CR value remained below 0.10 for each event, indicating

suitable and consistent weighting criteria (Bourenane et al. 2016; Pradhan and Kim, 2016). However, the AHP-based model has been criticized due to the expert-opinion-based subjective approach (Kumar et al. 2023; Ali et al. 2019. Hence, we performed spatial analysis to rate all causal factors to reduce the risks of inaccuracies associated with the cognitive limits of experts. All these factors were ranked based on the consistency ratio, suggesting that landslide in the study area is mainly related to steep slope regions followed by rainfall and earthquakes. Some seismic events and earthquake tremors cause rock to fall nearby and along the highway. Slope, rainfall, seismicity, and lithology have been considered highly rated.

In contrast, land cover and distances to streams, faults, and roads have less importance because of their poor linkage with landslide events in the study area. The results obtained from the FR technique were also used for the final construction of the LS map (Figure 6), representing the north, northwest, and northeast areas in a very highly susceptible zone. In contrast, the south and southwest sides lie in moderate to high susceptible zones. The AHP map also reflects the same susceptible zones.

Afterward, the ROC model was also applied to the FR technique, which revealed a value of 0.80 and AHP rated 0.73. The AUC values reported in this study imply satisfactory performance for both the AHP and FR approaches in landslide susceptibility mapping, according to the class ranges suggested for AUC interpretation (Hosmer et al. 2013). However, the FR method achieved slightly better than AHP. Therefore, the FR technique is a simple and easy way to value various parameters consistently, as evidenced in other previous works (Yilmaz, 2009; Park et al. 2013; Ding et al. 2017; Shana et al., 2018)

Meanwhile, some studies have reported a similar overall accuracy rate in models such as AHP and FR (Acharya and Lee, 2019). Hence, according to our research output, we conclude that the FR-based AUC model has better performance and reliable accuracy in determining landslide susceptibility across the study area.

5. Conclusions

This study developed a landslide susceptibility map of the Chitral region using GIS, integrating the Analytic Hierarchy Process (AHP) and Frequency Ratio (FR) methods. Nine controlling factors were weighted and analyzed: slope, lithology, faults, land cover, rainfall, seismicity, distance to roads, distance to streams, and slope aspect. The final landslide susceptibility map categorizes the region into five hazard zones, i.e. very low, low, moderate, high, and very high, with 73 % (AUC value) indicating satisfactory performance. Key findings reveal that slope is the dominant factor for triggering landslides, followed by rainfall and seismicity. The Reshun Fault and Main Karakoram Thrust are identified as high-risk seismic zones, where landslides frequently occur along the road networks passing by these faults. A Rockfall and debris slide along road sections are clear examples of active seismicity in the region. The susceptibility map is a valuable tool for effective mitigation and planning management, assisting in risk-informed infrastructure development, emergency response strategies, and resource allocation. First, the accuracy and reliability of the landslide susceptibility map should be enhanced by incorporating additional relevant datasets, exploring advanced techniques and models, and improving the mapping process. Future studies should enhance map accuracy by incorporating additional datasets, advanced modeling techniques, and field validation. Furthermore, integrating the susceptibility map into a comprehensive risk assessment framework will support the region's long-term landslide hazard management and mitigation strategies.

Acknowledgments:

We would like to express our gratitude to the Geological Survey of Pakistan, the Pakistan Meteorology Department, the USGS, and NASA for providing free data for this research.

Funding:

Authors receive no funding.

Conflicts of Interest:

The authors declare no conflict of interest.

References

Acharya, T. D., & Lee, D. H. (2019). Landslide susceptibility mapping using relative frequency and predictor rate along Araniko Highway. *KSCE Journal of Civil Engineering*, *23*, 763-776.

Agrawal, N., & Dixit, J. (2023). GIS-based landslide susceptibility mapping of the Meghalaya-Shillong Plateau region using machine learning algorithms. *Bulletin of Engineering Geology and the Environment*, *82*(5), 170.

Ahmad, M. N., Shao, Z., Aslam, R. W., Ahmad, I., Liao, M., Li, X., & Song, Y. (2022). Landslide hazard, susceptibility and risk assessment (HSRA) based on remote sensing and GIS data models: a case study of Muzaffarabad Pakistan. *Stochastic Environmental Research and Risk Assessment*, *36*(12), 4041-4056.

Ahmad, M. S., Lisa. M., & Khan, S. (2023). Comparative analysis of analytical hierarchy process (AHP) and frequency ratio (FR) models for landslide susceptibility mapping in Reshun, NW Pakistan. *Kuwait Journal of Science*, *50*(3), 387-398.

Ahmad, M. S., Lisa, M., & Khan, S. (2024). Assessment and mapping of landslides in steep mountainous terrain using PS-InSAR: A case study of Karimabad Valley in Chitral. *Kuwait Journal of Science*, *51*(1), 100137.

Ahmad, S. M., Sadhasivam, N., Lisa, M., Lombardo, L., Emil, M. K., Zaki, A., van Westen, C.J., Fadel, I., & Tanyas, H. (2024). Standing on the shoulder of a giant landslide: A six-year long InSAR look at a slow-moving hillslope in the western Karakoram. *Geomorphology*, *444*, 108959.

Ahmed, B. (2015). Landslide susceptibility mapping using multi-criteria evaluation techniques in Chittagong Metropolitan Area, Bangladesh. *Landslides*, *12*(6), 1077-1095.

Ali, S., Biermanns, P., Haider, R., & Reicherter, K. (2019). Landslide susceptibility mapping by using a geographic information system (GIS) along the China–Pakistan Economic Corridor (Karakoram Highway), Pakistan. *Natural Hazards and Earth System Sciences*, *19*(5), 999-1022.

Aneel, A., Nasrullah, A., Khalid, S., Xuan, X. X., Ahmad, S. M., & Ning, S. (2023). Landslide susceptibility mapping of Chilas area along Karakorum highway, Gilgit Baltistan, Pakistan. *Iranian Journal of Geophysics, 16*(4), 69-84.

Aslam, B., Zafar, A., & Khalil, U. (2023). Comparative analysis of multiple conventional neural networks for landslide susceptibility mapping. *Natural Hazards*, *115*(1), 673-707.

Bachri, S., & Shresta, R. P. (2010). Landslide hazard assessment using analytic hierarchy processing (AHP) and geographic information system in Kaligesing mountain area of Central Java Province Indonesia.

Basharat, M., Shah, H. R., & Hameed, N. (2016). Landslide susceptibility mapping using GIS and weighted overlay method: a case study from NW Himalayas, Pakistan. *Arabian Journal of Geosciences*, *9*, 1-19.

Boukhres, N., Mastere, M., Thiery, Y., Maquaire, O., El Fellah, B., & Costa, S. (2023). A comparative modeling of landslides susceptibility at a meso-scale using frequency ratio and analytic hierarchy process models in geographic information system: the case of African Alpine Mountains (Rif, Morocco). *Modeling Earth Systems and Environment*, *9*(2), 1949-1975.

Bourenane, H., Guettouche, M. S., Bouhadad, Y., & Braham, M. (2016). Landslide hazard mapping in the Constantine city, Northeast Algeria using frequency ratio, weighting factor, logistic regression, weights of evidence, and analytical hierarchy process methods. *Arabian Journal of Geosciences*, *9*, 1-24.

Dai, F. C., Lee, C. F., Li, J. X. Z. W., & Xu, Z. W. (2001). Assessment of landslide susceptibility on the natural terrain of Lantau Island, Hong Kong. *Environmental geology*, *40*, 381-391.

Das, Suvam, Shantanu Sarkar, and Debi Prasanna Kanungo. "GIS-based landslide susceptibility zonation mapping using the analytic hierarchy process (AHP) method in parts of Kalimpong Region of Darjeeling Himalaya." *Environmental Monitoring and Assessment* 194.4 (2022): 234.

Ding, Q., Chen, W., & Hong, H. (2017). Application of frequency ratio, weights of evidence and evidential belief function models in landslide susceptibility mapping. *Geocarto international*, *32*(6), 619-639.

Du, J., Glade, T., Woldai, T., Chai, B., & Zeng, B. (2020). Landslide susceptibility assessment based on an incomplete landslide inventory in the Jilong Valley, Tibet, Chinese Himalayas. *Engineering Geology*, *270*, 105572.

Fraser, J. E., Searle, M. P., Parrish, R. R., & Noble, S. R. (2001). Chronology of deformation, metamorphism, and magmatism in the southern Karakoram Mountains. *Geological Society of America Bulletin*, *113*(11), 1443-1455.

Ghimire, M. (2011). Landslide occurrence and its relation with terrain factors in the Siwalik Hills, Nepal: case study of susceptibility assessment in three basins. *Natural hazards*, *56*(1), 299-320.

Gorsevski, P. V., Gessler, P. E., Foltz, R. B., & Elliot, W. J. (2006). Spatial prediction of landslide hazard using logistic regression and ROC analysis. *Transactions in GIS*, *10*(3), 395-415.

Guzzetti, F., Gariano, S. L., Peruccacci, S., Brunetti, M. T., Marchesini, I., Rossi, M., & Melillo, M. (2020). Geographical landslide early warning systems. *Earth-Science Reviews*, *200*, 102973.

Guzzetti, F., Mondini, A. C., Cardinali, M., Fiorucci, F., Santangelo, M., & Chang, K. T. (2012). Landslide inventory maps: New tools for an old problem. *Earth-Science Reviews*, *112*(1-2), 42-66.

Hildebrand, P. R., Noble, S. R., Searle, M. P., Waters, D. J., & Parrish, R. R. (2001). Old origin for an active mountain range: Geology and geochronology of the eastern Hindu Kush, Pakistan. *Geological Society of America Bulletin*, *113*(5), 625-639.

Hosmer Jr, D. W., Lemeshow, S., & Sturdivant, R. X. (2013). *Applied logistic regression*. John Wiley & Sons.

Kaur, H., Gupta, S., Parkash, S., & Thapa, R. (2023). Knowledge-driven method: a tool for landslide susceptibility zonation (LSZ). *Geology, Ecology, and Landscapes*, *7*(1), 1-15.

Khan, A., Gupta, S., & Gupta, S. K. (2020). Multi-hazard disaster studies: Monitoring, detection, recovery, and management, based on emerging technologies and optimal techniques. *International journal of disaster risk reduction*, *47*, 101642.

Khan, M. A., Treloar, P. J., Searle, M. P., & Jan, M. Q. (2000). Tectonics of the Nanga Parbat Syntaxis and the Western Himalaya. Geological Society of London.

Khattak, G. A., Owen, L. A., Kamp, U., & Harp, E. L. (2010). Evolution of earthquake-triggered landslides in the Kashmir Himalaya, northern Pakistan. *Geomorphology*, *115*(1-2), 102-108.

Kumar, M., Biswas, S., Kar, S., Božanić, D., & Puška, A. (2023). An Interval Type 2 Fuzzy Decision-Making Framework for Exploring Critical Issues for the Sustenance of the Tea Industry. *Axioms*, *12*(10), 986.

Kuradusenge, M., Kumaran, S., & Zennaro, M. (2020). Rainfall-induced landslide prediction using machine learning models: The case of Ngororero District, Rwanda. *International journal of environmental research and public health*, *17*(11), 4147.

Mao, Y., Li, Y., Teng, F., Sabonchi, A. K., Azarafza, M., & Zhang, M. (2024). Utilizing hybrid machine learning and soft computing techniques for landslide susceptibility mapping in a Drainage Basin. *Water*, *16*(3), 380.

Panday, S., & Dong, J. J. (2021). Topographical features of rainfall-triggered landslides in Mon State, Myanmar, August 2019: Spatial distribution heterogeneity and uncommon large relative heights. *Landslides*, *18*(12), 3875-3889.

Park, D. W., Nikhil, N. V., & Lee, S. R. (2013). Landslide and debris flow susceptibility zonation using TRIGRS for the 2011 Seoul landslide event. *Natural Hazards and Earth System Sciences*, *13*(11), 2833-2849.

Pradhan, A. M. S., & Kim, Y. T. (2016). Evaluation of a combined spatial multi-criteria evaluation model and deterministic model for landslide susceptibility mapping. *Catena*, *140*, 125-139.

Ray, R. L., Lazzari, M., & Olutimehin, T. (2020). Remote sensing approaches and related techniques to map and study landslides. *Landslides-Investig. Monit*, *2*, 1-25.

Razavizadeh, S., Solaimani, K., Massironi, M., & Kavian, A. (2017). Mapping landslide susceptibility with frequency ratio, statistical index, and weights of evidence models: a case study in northern Iran. *Environmental Earth Sciences*, *76*, 1-16.

Regmi, A. D., Devkota, K. C., Yoshida, K., Pradhan, B., Pourghasemi, H. R., Kumamoto, T., & Akgün, A. (2014). Application of frequency ratio, statistical index, and weights-of-evidence models and their comparison in landslide susceptibility mapping in Central Nepal Himalaya. *Arabian Journal of Geosciences*, *7*, 725-742.

ReliefWeb. 2024. *Floods Rapid Needs Analysis Report 2024 Chitral, Pakistan*. Geneva, Switzerland: United Nations Office for the Coordination of Humanitarian Affairs (OCHA). Retrieved February 7, 2025 (https://reliefweb.int/report/pakistan/floods-rapid-needs-analysis-report-2024-chitral-pakistan).

Saha, S., Majumdar, P., & Bera, B. (2023). Deep learning and benchmark machine learning based landslide susceptibility investigation, Garhwal Himalaya (India). *Quaternary Science Advances*, *10*, 100075.

Saleem, M., Naseem, A.A., Rehman, F. *et al.* Satellite-based lithological characterization of Central Chitral, Karakoram Ranges, Northern Pakistan. *Arab J Geosci* 14, 1000 (2021). https://doi.org/10.1007/s12517-021-07350-6

Schurr, B., Ratschbacher, L., Sippl, C., Gloaguen, R., Yuan, X., & Mechie, J. (2014). Seismotectonics of the Pamir. *Tectonics*, *33*(8), 1501-1518.

Tang, Y., Feng, F., Guo, Z., Feng, W., Li, Z., Wang, J., Sun, Q., Ma, H., & Li, Y. (2020). Integrating principal component analysis with statistically-based models for analysis of causal factors and landslide susceptibility mapping: A comparative study from the loess plateau area in Shanxi (China). *Journal of Cleaner Production*, *277*, 124159.

Thapa, D., & Bhandari, B. P. (2019). GIS-Based frequency ratio method for identification of potential landslide susceptible area in the Siwalik zone of Chatara-Barahakshetra section, Nepal. *Open Journal of Geology*, *9*(12), 873.

Vakhshoori, V., & Zare, M. (2018). Is the ROC curve a reliable tool to compare the validity of landslide susceptibility maps?. *Geomatics, Natural Hazards and Risk*, *9*(1), 249-266.

Van Westen, C. J., Van Asch, T. W., & Soeters, R. (2006). Landslide hazard and risk zonation—why is it still so difficult?. *Bulletin of Engineering geology and the Environment*, *65*, 167-184.

Wang, Y., Chai, J., Cao, J., Qin, Y., Xu, Z., & Zhang, X. (2020). Effects of seepage on a three-layered slope and its stability analysis under rainfall conditions. *Natural Hazards*, *102*, 1269-1278.

Wang, G., Chen, X., & Chen, W. (2020). Spatial prediction of landslide susceptibility based on GIS and discriminant functions. *ISPRS International Journal of Geo-Information*, *9*(3), 144.

Wu, Q., Xie, Z., Tian, M., Qiu, Q., Chen, J., Tao, L., & Zhao, Y. (2024). Integrating Knowledge Graph and Machine Learning Methods for Landslide Susceptibility Assessment. *Remote Sensing*, *16*(13), 2399.

Xu, Q., Zhao, B., Dai, K., Dong, X., Li, W., Zhu, X., Yang. Y., Xiao, X., Wang, X, Huang, J., Lu, H., Deng, B., & Ge, D. (2023). Remote sensing for landslide investigations: A progress report from China. *Engineering Geology*, *321*, 107156.

Yalçın, A., Reis, S., Aydınoğlu, A. C., & Yomralioglu, T. (2011). A GIS-based comparative study of frequency ratio, analytical hierarchy process, bivariate statistics and logistics regression methods for landslide susceptibility mapping in Trabzon, NE Turkey. *Catena*, *85*(3), 274-287.

Yeşilnacar, E., & Hunter, G. J. (2005). Application of neural networks for landslide susceptibility mapping in Turkey. In *Recent advances in design and decision support systems in architecture and urban planning* (pp. 3-18). Springer Netherlands.

Yılmaz, I. (2009). Landslide susceptibility mapping using frequency ratio, logistic regression, artificial neural networks and their comparison: a case study from Kat landslides (Tokat—Turkey). *Computers & Geosciences*, *35*(6), 1125-1138.

Youssef, B., Bouskri, I., Brahim, B., Kader, S., Brahim, I., Abdelkrim, B., & Spalević, V. (2023). The contribution of the frequency ratio model and the prediction rate for the analysis of landslide risk in the Tizi N'tichka area on the national road (RN9) linking Marrakech and Ouarzazate. *Catena*, *232*, 107464.

Zanchi, A., Poli, S., Fumagalli, P., & Gaetani, M. (2000). Mantle exhumation along the Tirich Mir Fault Zone, NW Pakistan: pre-mid-Cretaceous accretion of the Karakoram terrane to the Asian margin. *Geological Society, London, Special Publications*, *170*(1), 237-252.

Zêzere, J. L., Pereira, S., Melo, R., Oliveira, S. C., & Garcia, R. A. (2017). Mapping landslide susceptibility using data-driven methods. *Science of the total environment*, *589*, 250-267.

Zhang, W., Liu, S., Wang, L., Samui, P., Chwała, M., & He, Y. (2022). Landslide susceptibility research combining qualitative analysis and quantitative evaluation: A case study of Yunyang County in Chongqing, China. *Forests*, *13*(7), 1055.

Zhang, Y. X., Lan, H. X., Li, L. P., Wu, Y. M., Chen, J. H., & Tian, N. M. (2020). Optimizing the frequency ratio method for landslide susceptibility assessment: A case study of the Caiyuan Basin in the southeast mountainous area of China. *Journal of Mountain Science*, *17*(2), 340-357.

Zou, Q., Jiang, H., Cui, P., Zhou, B., Jiang, Y., Qin, M., ... & Li, C. (2021). A new approach to assess landslide susceptibility based on slope failure mechanisms. *Catena*, *204*, 105388.

Zulhaidi Mohd Shafri, H., Mohd Zahidi, I., & Abu Bakar, S. (2010). Development of landslide susceptibility map utilizing remote sensing and Geographic Information Systems (GIS). *Disaster Prevention and Management: An International Journal*, *19*(1), 59-69.